

Dynamic metal along grain boundaries in Floquet topological crystals

Daniel J. Salib¹ and Bitan Roy¹

¹*Department of Physics, Lehigh University, Bethlehem, Pennsylvania, 18015, USA*

(Dated: December 16, 2022)

Driven quantum materials often feature emergent topology, otherwise absent in static crystals. Dynamic bulk-boundary correspondence, encoded by nondissipative gapless modes residing near the Floquet zone center and/or boundaries, is the most prominent example of such phenomena. Here we show that topologically robust gapless metallic states appear along the grain boundaries, embedded in the interior of Floquet topological crystals, when the Floquet-Bloch band inversion occurring at a finite momentum ($\mathbf{K}_{\text{inv}}^{\text{Flq}}$) and the Burgers vector (\mathbf{b}) of the constituting array of dislocations satisfy $\mathbf{K}_{\text{inv}}^{\text{Flq}} \cdot \mathbf{b} = \pi$ (modulo 2π). Such dissipationless metallic states can be found near the center and/or edge of the Floquet Brillouin zone, irrespective of the drive protocol. We showcase these general outcomes for two-dimensional driven time-reversal symmetry breaking insulators. Promising experimental platforms, unveiling such dynamic topological metals in real materials, are discussed.

Introduction. Defects are ubiquitous in crystals, such as dislocations and grain boundaries. They are responsible for crystal melting that takes place through proliferation of lattice defects, which can be either pointlike, such as edge dislocations in two-dimensional (2D) crystals or extended, such as screw dislocations and grain boundaries. Furthermore, line defects can often be constructed by stacking point defects. For example, an array of edge dislocations gives rise to a grain boundary [1]. In recent time, such geometric lattice defects have gained a revived interest in the context of topological quantum materials [2, 3]. Under conducive environments, they can harbor robust topological modes in their vicinity that are, most importantly, immune to interface contamination [4–21]. As lattice defects locally break the translational symmetry in the bulk of crystals, topological phases harboring such defect modes are thus named translationally active. While lattice defects in static topological materials have been scrutinized thoroughly over the span of last few years, their role as smoking gun probe of dynamic topological phases is still at its infancy [15, 20].

Here we showcase emergence of one-dimensional (1D) dynamic topological metals along the grain boundary of a 2D Floquet topological crystal. For simplicity, we consider a system that in the static limit features both topological insulators (TIs) and atomic or normal insulators (NIs) at the cost of the time-reversal symmetry. In particular, when the band inversion of the TI takes place at a momentum \mathbf{K}_{inv} in the Brillouin zone such that along with the Burgers vector of the underlying constituting dislocation \mathbf{b} , it satisfies $\mathbf{K}_{\text{inv}} \cdot \mathbf{b} = \pi$ (modulo 2π), 1D gapless metallic states appear along the grain boundary [11]. They form a metallic miniband within the bulk topological band gap along the line defect. See Fig. 1.

Irrespective of the periodic drive protocol, we show that such a system features a plethora of topological and normal insulating phases in the dynamic realm even when its static counterpart describes a NI, imprinted within the corresponding global phase diagrams shown in Fig. 2, depending on the drive frequency (ω) and its amplitude.

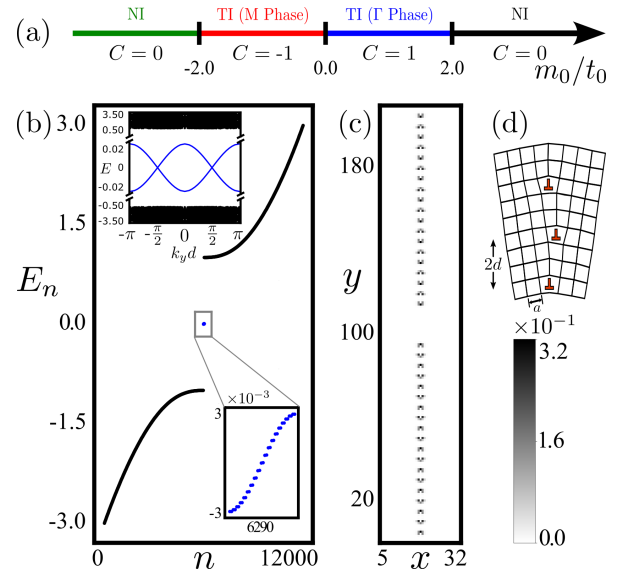


FIG. 1: (a) Phase diagram of the static Hamiltonian H_{stat} [Eq. (1)] in terms of the Chern number (C) [Eq. (3)]. (b) Energy spectra of H_{stat} in a periodic system with a pair of grain-antigrain boundary each containing 10 (anti)dislocations, with the Burgers vector $\mathbf{b} = \pm a \hat{e}_1$ for $t = t_0 = 1$ and $m_0 = -1.5$, such that the system is in the translationally active M phase. One-dimensional metallic states (blue dots in lower inset) then appear along the line defects, as can be seen from their Fourier transformation as a function of the conserved momentum k_y (upper inset). (c) Local density of states of these modes is highly localized along the line defects. (d) An illustration of a grain boundary with three dislocations. Their cores are shown in red. Throughout, the distance between two successive dislocation cores is $2d$.

The time translational symmetry then gives birth to the Floquet Brillouin zone (FBZ) within the quasienergy $\mu \in (-\omega/2, \omega/2)$ [22–26]. As a result, the inversion of the Floquet-Bloch bands, taking place at spatial momentum $\mathbf{K}_{\text{inv}}^{\text{Flq}}$, can occur near the FBZ center and/or near its boundaries. Under this circumstance, the $\mathbf{K} \cdot \mathbf{b}$ rule for

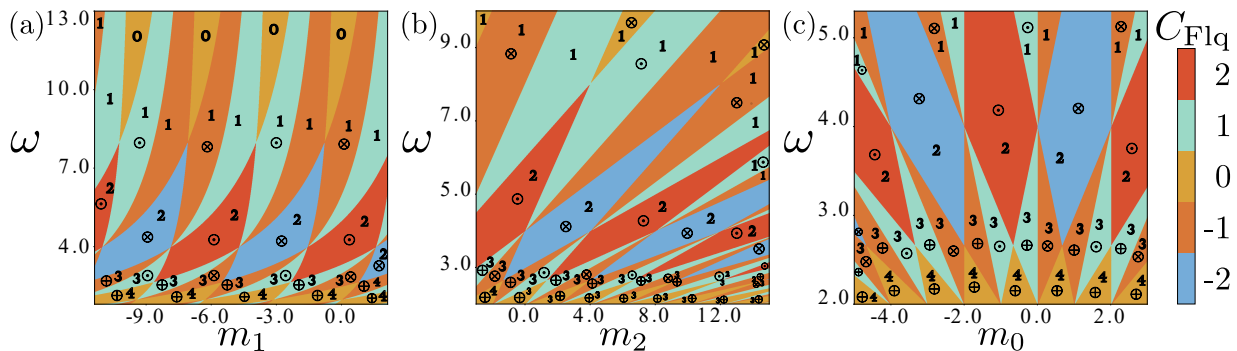


FIG. 2: Global phase diagrams of time reversal odd insulators, subject to (a) kick [Eq. (4)], (b) step [Eq. (5)] and (c) sinusoidal [Eq. (6)] drives. Here ω is the drive frequency. Phases are colored (numbered) according to the Floquet Chern number C_{Flq} (number of total edge modes in the Floquet Brillouin zone or winding number \mathcal{W} [24]). Insulators supporting normal, anomalous and mixed (with both normal and anomalous) one-dimensional dynamic metals along the grain boundary are marked by \odot , \otimes and \oplus , respectively. See Figs. 3-5 [27]. Here we set $t = t_0 = 1$, and (a) $m_0 = 3$, (b) $m_0 = 3$, $m_1 = m_3 = 2$, and (c) $V = 3$.

the metallic grain boundary extends to dynamic systems, but in terms of $\mathbf{K}_{\text{inv}}^{\text{Flq}}$. And we display the appearance of nondissipative (a) normal 1D dynamic metals around the FBZ center and zero quasienergy, (b) anomalous 1D dynamic metals around the FBZ boundaries and quasienergies $\pm\omega/2$, and (c) mixed 1D dynamic metals, simultaneously featuring both normal and anomalous dynamic metals along the grain boundary. These generic outcomes are explicitly shown for the kick [Fig. 3], step [Fig. 4] and periodic [Fig. 5] drives. They are qualitatively similar for small angle grain boundaries (SAGBs) and their large angle counterparts. Results for the latter are relegated to the Supplemental Materials (SM) [27].

Model. A pedagogical discussion on the static system and grain boundaries therein will benefit the forthcoming discussion on the role of such line defects in Floquet topological insulators. The Hamiltonian for the static system is given by $H_{\text{stat}} = \boldsymbol{\tau} \cdot \mathbf{d}(\mathbf{k})$, where [28]

$$\mathbf{d}(\mathbf{k}) = \left(t \sin(k_x a), t \sin(k_y a), m_0 - t_0 \sum_{j=x,y} \cos(k_j a) \right), \quad (1)$$

with \mathbf{k} as spatial momenta and a as the lattice spacing. Vector Pauli matrix $\boldsymbol{\tau}$ operates on orbitals. This model supports TIs (NIs) within the parameter range $|m_0/t_0| < 2$ ($|m_0/t_0| > 2$). Within the topological regime, the inversion of the Bloch bands (\mathbf{K}_{inv}) takes place near the $\Gamma = (0,0)$ and the $M = (1,1)\pi/a$ points of the Brillouin zone for $0 < m_0/t_0 < 2$ and $-2 < m_0/t_0 < 0$, respectively, and named the Γ phase and M phase. The band inversion momentum can be recognized from the band structure of H_{stat} in a semi-infinite system with k_x or k_y as good quantum number. The edge modes then cross the zero energy at momentum \mathbf{K}_{inv} [27]. These two TIs are characterized by distinct first Chern number (C) computed in the following way [29, 30].

We consider a discrete 2D Brillouin zone, containing

reciprocal lattice points $\mathbf{k}_\ell = (k_{j_1}, k_{j_2})$, where $k_{j_\mu} = (2\pi j_\mu / N_\mu) - \pi$, $j_\mu = 0, \dots, N_\mu - 1$ and $\mu = 1, 2$. For simplicity, here we take $N_1 = N_2 = N$. The Brillouin zone is restricted within $|k_{j_\mu}| < \pi$. A $U(1)$ link variable for $\mathbf{k}_\ell \rightarrow \mathbf{k}_\ell + \hat{\boldsymbol{\mu}}$ is defined as $U_\mu(\mathbf{k}_\ell) \equiv \langle n(\mathbf{k}_\ell) | n(\mathbf{k}_\ell + \hat{\boldsymbol{\mu}}) \rangle / A$, where $|n(\mathbf{k}_\ell)\rangle$ is the normalized eigenstate of band n of H_{stat} at momentum \mathbf{k}_ℓ , $A = |\langle n(\mathbf{k}_\ell) | n(\mathbf{k}_\ell + \hat{\boldsymbol{\mu}}) \rangle|$ and $\hat{\boldsymbol{\mu}} = (2\pi/N)\hat{\mathbf{e}}_\mu$. A counter-clockwise path around a unit plaquette in the reciprocal space is then represented by

$$P_{12}(\mathbf{k}_\ell) = U_1(\mathbf{k}_\ell) U_2(\mathbf{k}_\ell + \hat{\mathbf{1}}) U_1(\mathbf{k}_\ell + \hat{\mathbf{2}})^{-1} U_2(\mathbf{k}_\ell)^{-1}, \quad (2)$$

yielding lattice field strength $F_{12}(\mathbf{k}_\ell) = \ln P_{12}(\mathbf{k}_\ell)$ with $-\pi \leq -iF_{12}(\mathbf{k}_\ell) \leq \pi$. The corresponding Chern number

$$C_n = \frac{1}{2\pi i} \sum_{\ell} F_{12}(\mathbf{k}_\ell) \quad (3)$$

typically converges for $N = 30$. Throughout, we compute it for the valence band and set $C_n = C$ for brevity, leading to $C = +1$ (-1) in the Γ (M) phase.

When an edge dislocation is introduced in an otherwise square lattice system through the Volterra cut-and-paste procedure, the electron encircling the core of such lattice defect picks up a hopping phase $\Phi_{\text{dis}} = \mathbf{K}_{\text{inv}} \cdot \mathbf{b}$ (modulo 2π). The Burgers vector \mathbf{b} measures the missing translation around the defect core across the line of missing atoms, and here we take $\mathbf{b} = a\hat{\mathbf{e}}_1$. Then, in the M phase $\Phi_{\text{dis}} = \pi$, while $\Phi_{\text{dis}} = 0$ in the Γ phase. Thus only in the M phase a nontrivial π -flux threads through the dislocation core and the system supports a zero energy localized topological mode in its close vicinity [7].

Once a grain boundary is created from the array of such edge dislocations, tunneling among the zero energy modes bound to each dislocation core causes hybridization among them. As a result, a 1D metallic miniband develops within and separated from the bulk band gap [11]. Such a 1D topological metal resides along the

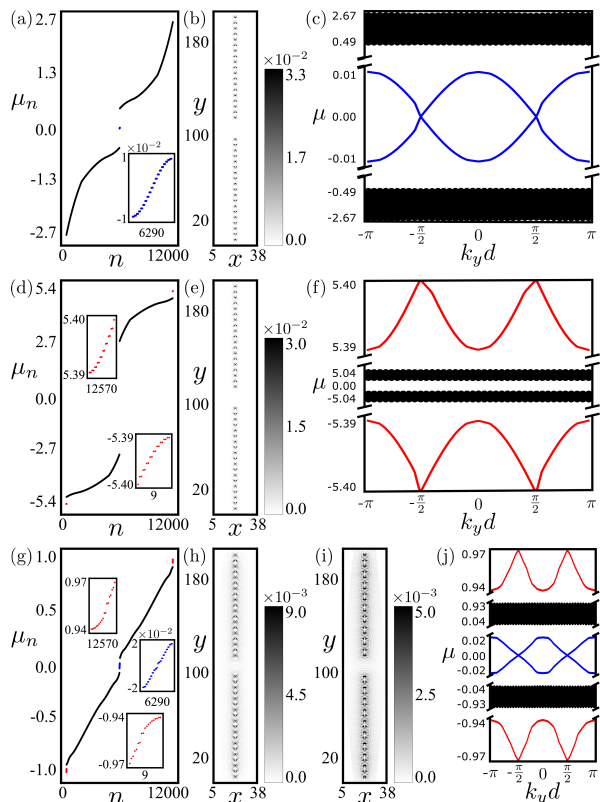


FIG. 3: Dynamic metals along the grain-antigrain boundary stemming from a kick drive [Eq. (4)]. (a) Quasienergy (μ) spectra in a system with periodic boundary conditions and a grain-antigrain boundary pair, each containing 10 (anti)dislocations, for $\omega = 12.8$, $m_1 = -1.8$ producing a normal dynamic metal near the Floquet zone center (blue dots). (b) Their local density of states (LDOS) is highly localized along the line defects. (c) Fourier transformation of the same set of states confirms their metallic nature. Panels (d), (e) and (f) are similar to (a), (b) and (c), respectively, however for $\omega = 10.8$, $m_1 = -5.2$ giving rise to an anomalous dynamic metal (red dots) near the Floquet zone boundary. Panel (g) is similar to (a), but for $\omega = 1.94$, $m_1 = -4.5$ hosting both normal (blue) and anomalous (red) metallic states, for which the LDOS are respectively shown in (h) and (i). (j) Fourier transformation pins their metallic nature near the Floquet zone center and boundary. We set $m_0 = 3$ and $t = t_0 = 1$.

grain boundary. Their gapless nature can be anchored from the corresponding Fourier transformation in terms of the conserved momentum k_y along the grain boundary for $\mathbf{b} = a\hat{\mathbf{e}}_1$. When the dislocation modes hybridize, the metallic states besides maintaining high localization at the defect core also develop comparable spectral weight in between them. For this reason, while performing their Fourier transformation, we denote the distance between two successive defect cores by $2d$. These results are summarized in Fig. 1. The grain boundary is characterized by the angle $\theta = \sin^{-1}(a/d)$. For SAGBs we set $d = 5a$, yielding $\theta = 11.54^\circ < 15^\circ$.

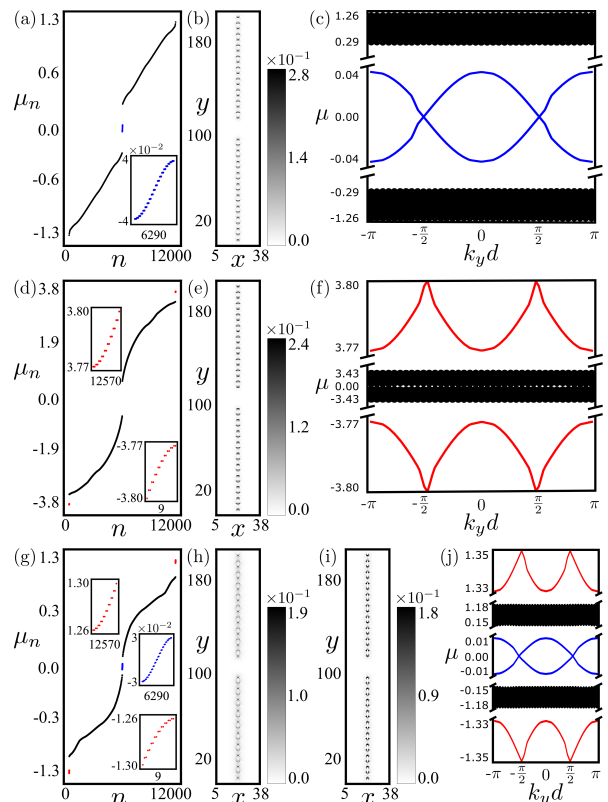


FIG. 4: Dynamic metals along the grain-antigrain boundary with a step drive [Eq. (5)]. (a) Quasienergy (μ) spectra in a system with a grain-antigrain boundary pair, each containing 10 (anti)dislocations, and periodic boundary conditions for $\omega = 3.5$, $m_2 = -2.5$ producing a normal dynamic metal near the Floquet zone center (blue dots). (b) Their local density of states (LDOS) displays strong localization along the line defects. (c) Fourier transformation of the same set of states, confirming their metallic nature. Panels (d), (e) and (f) are similar to (a), (b) and (c), respectively, however for $\omega = 7.6$, $m_2 = -2.8$ supporting an anomalous dynamic metal (in red) near the Floquet zone boundary. (g) is similar to (a), but for $\omega = 2.7$, $m_2 = -2.9$ hosting both normal (blue) and anomalous (red) metallic states, whose LDOS are respectively shown in (h) and (i). (j) Their Fourier transformation shows metallic nature near both the Floquet zone center and boundary. Here we set $m_0 = 3$, $m_1 = m_3 = 2$ and $t = t_0 = 1$.

Driven system. With the stage being set, we now focus on the same system under periodic drives. In particular, here we consider three drives. (a) A kick drive with

$$V(t) = m_1\tau_3 \sum_{n=-\infty}^{\infty} \delta(t - nT) \quad (4)$$

where n is an integer, (b) a step drive given by

$$V(t) = \begin{cases} m_1\tau_3 & nT < t < nT + T/4, \\ m_2\tau_3 & nT + T/4 < t < nT + 3T/4, \\ m_3\tau_3 & nT + 3T/4 < t < (n+1)T, \end{cases} \quad (5)$$

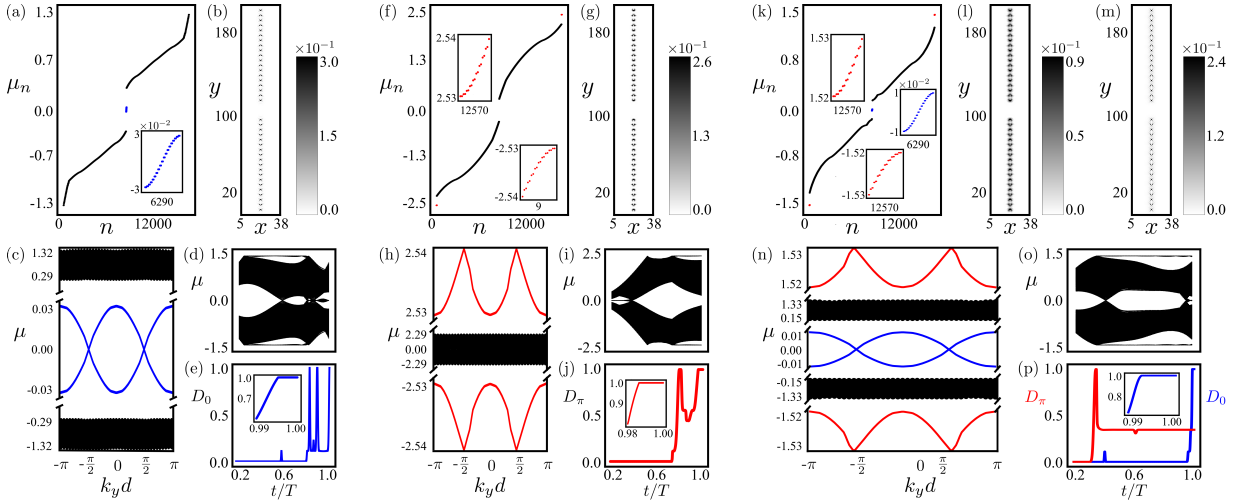


FIG. 5: Dynamic metals along the grain-antigrain boundary with a sinusoidal drive [Eq. (6)]. (a) Quasienergy (μ) spectra in a system with periodic boundary conditions and a grain-antigrain boundary pair, each containing 10 (anti)dislocations, for $\omega = 3.10$, $m_0 = 2.42$, yielding a normal metal near the Floquet zone center (blue dots). Their (b) local density of states (LDOS) is highly localized along the line defects and (c) Fourier transform depicts the metallic nature. Time evolution of (d) quasienergy spectra and (e) normalized density of states (NDOS) near Floquet zone center (D_0) in a system with 5 (anti)dislocations forming the grain-antigrain boundary pair for the same parameters as in (a). Panels (f)-(j) are similar to (a)-(e), respectively, but for $\omega = 5.08$, $m_0 = -2.79$, producing an anomalous (red) metal along the line defects. Here D_π denotes the NDOS near the Floquet zone boundary. Panel (k) is similar to (a), but for $\omega = 3.06$, $m_0 = 1.33$, giving rise to both normal (blue) and anomalous (red) metals along the line defects. Their LDOS are respectively shown in (l) and (m), while (n) Fourier transformation shows metallic nature near both the Floquet zone center and boundary. Time evolution of (o) quasienergy spectra and (p) NDOS near the Floquet zone center (blue) and boundary (red) in a system as in (d). We set $V = 3$ and $t = t_0 = 1$.

where we set $m_1 = m_3$, and (c) a sinusoidal drive

$$V(t) = V \cos(2\pi t/T) \tau_3. \quad (6)$$

The drive frequency is $\omega = 2\pi/T$. The corresponding time ordered (TO) Floquet unitary operator is

$$U(\mathbf{k}, t) = \text{TO} \left(\exp \left[-i \int_0^t [H_{\text{stat}}(\mathbf{k}) + V(t)] dt \right] \right). \quad (7)$$

For sinusoidal drive $U(\mathbf{k}, t)$ is computed employing the Trotter-Suzuki approximation [31, 32]. We are mostly interested at the stroboscopic time $t = T$, at which the effective Floquet Hamiltonian is given by

$$H_{\text{Flq}}(\mathbf{k}) = i \ln(U(\mathbf{k}, T))/T = \mathbf{d}_{\text{Flq}}(\mathbf{k}, T) \cdot \boldsymbol{\tau}. \quad (8)$$

The explicit form of $\mathbf{d}_{\text{Flq}}(\mathbf{k}, T)$ is shown in the SM [27]. The global phase diagram of such a system can be constructed in terms of the Chern number for $H_{\text{Flq}}(\mathbf{k})$, employing the method discussed earlier for H_{stat} . See Fig. 2.

When periodically driven, inversion of the Floquet-Bloch bands can then take place near the center and/or boundaries of the FBZ. Recall, a static TI with the band inversion at the Γ (M) point leads to $C = +1$ (-1). The same conclusions hold for the Floquet insulators when the band inversion occurs near the FBZ center. By contrast, the correspondence between the Chern number and band inversion momentum gets reversed when it happens

near the boundaries of the FBZ. The net Chern number for Floquet insulators is given by $C_{\text{Flq}} = C_{\text{FZC}} + C_{\text{FZB}}$, where C_{FZC} (C_{FZB}) denotes the Chern number stemming from the FBZ center (boundaries). Therefore, combinations of C_{FZC} and C_{FZB} yield a myriad Floquet insulators with integer C_{Flq} ranging from -2 to 2 [Fig. 2], even though its static counterpart only permits insulators with $C = 0, \pm 1$ [Fig. 1]. Consequently, it is then conceivable to find trivial Floquet insulators with $C_{\text{Flq}} = 0$, which support topological edge modes at same momentum near the center and boundaries of the FBZ.

In Floquet insulators, nondissipative edge modes cross zero and/or $\pm\omega/2$ quasienergies at the Floquet-Bloch band inversion momentum ($\mathbf{K}_{\text{inv}}^{\text{Flq}}$) when it occurs at the FBZ center and/or boundaries, respectively. It can be anchored from the band structure of the time evolution operator $U(\mathbf{k}, T)$ in a semi-infinite system with k_x or k_y as a good quantum number in terms of its eigenmodes $|\mu_n\rangle$ with quasienergy μ_n , together satisfying $U(\mathbf{k}, T)|\mu_n\rangle = \exp(i\mu_n T)|\mu_n\rangle$ [27]. Notice that the global phase diagrams [Fig. 2] support insulators with identical C_{Flq} and total number of edge modes (set by the winding number \mathcal{W} [24]) that respond distinctly to translational symmetry breaking in the bulk of a Floquet crystal (sensitive to $\mathbf{K}_{\text{inv}}^{\text{Flq}}$) realized by introducing dislocations or grain boundaries in the system. Therefore, together the Floquet Charge number, winding number and

responses to grain boundaries, a direct probe of $\mathbf{K}_{\text{inv}}^{\text{Flq}}$, provide a complete classification of Floquet insulators.

The requisite topological criteria for the existence of 1D dynamic metallic states along the grain boundary in Floquet crystals extends directly from its counterpart in static systems. For example, when the Floquet-Bloch band inversion occurs at the Floquet zone center (boundary), normal (anomalous) dynamic 1D metals appear along such line defects around zero ($\pm\omega/2$) quasienergy. On the other hand, when the Floquet-Bloch band inversion occurs near the center and boundaries of the FBZ simultaneously, grain boundaries harbor mixed 1D dynamic metallic states, an admixture of both normal and anomalous metallic states. These outcomes are insensitive to the drive protocol. We arrive at qualitatively similar outcomes for the kick [Fig. 3], step [Fig. 4] and sinusoidal [Fig. 5] drives. Although, here we present these results for SAGBs, qualitatively similar conclusions hold for large angle grain boundaries as well [27]. In all these cases, the static system corresponds to a NI, such that the emergence of 1D dynamic metallic grain boundary modes can solely be attributed to the periodic drives.

Discussions. To summarize, here we show that irrespective of the drive protocol, Floquet insulators accommodate topologically robust one-dimensional gapless metallic states along grain boundaries whenever inversion of the underlying Floquet-Bloch bands takes place at a finite momentum ($\mathbf{K}_{\text{inv}}^{\text{Flq}}$) that together with the Burgers vector of the constituting dislocations (\mathbf{b}) satisfies $\mathbf{K}_{\text{inv}}^{\text{Flq}} \cdot \mathbf{b} = \pi$ (modulo 2π) [Fig. 2]. Otherwise, such dissipationless metallic states appear near zero and/or $\pm\omega/2$ quasienergies when in our model $\mathbf{K}_{\text{inv}}^{\text{Flq}} = (\pi, \pi)/a$ near the Floquet zone center and/ or boundary. These conclusions hold for both small angle [Figs. 3- 5] as well as large angle grain boundaries [27]. Furthermore, our findings rests on a robust topological criterion and therefore should naturally be applicable to driven systems belonging to arbitrary symmetry class in arbitrary dimensions.

With the recent progress in engineering Floquet topological phases in quantum crystals [33], cold atomic lattices [34, 35] and dynamic metamaterials [36–41] our proposal should be within the reach of currently achievable experimental setups, where dislocation lattice defects [12, 13] as well as grain boundaries [42] have already been demonstrated as tools to detect topological phases of matter in terms of robust modes bound to them. While defects are ubiquitous in quantum crystals, they can be engineered externally by suitably arranging optical waveguides [43] and mechanical resonators [44] in photonic and mechanical lattices, respectively. The LDOS of the grain boundary modes can be detected via scanning tunneling microscope in quantum crystals, two point pump probe or reflection spectroscopy in photonic lattices and mechanical susceptibility in acoustic lattices.

Acknowledgments. This work was supported by a

Startup grant of B.R. from Lehigh University. B.R. is thankful to Vladimir Juričić for discussions.

-
- [1] P. Chaikin and T. C. Lubensky, *Principles of Condensed Matter Physics* (Cambridge University Press, Cambridge, UK, 2000).
 - [2] M. Z. Hasan and C. L. Kane, Rev. Mod. Phys. **82**, 3045 (2010).
 - [3] X.-L. Qi and S. C. Zhang, Rev. Mod. Phys. **83**, 1057 (2011).
 - [4] Y. Ran, Y. Zhang, and A. Vishwanath, Nat. Phys. **5**, 298 (2009).
 - [5] J. C. Y. Teo and C. L. Kane, Phys. Rev. B **82**, 115120 (2010).
 - [6] D. Asahi and N. Nagaosa, Phys. Rev. B **86**, 100504(R) (2012).
 - [7] V. Juričić, A. Mesaros, R.-J. Slager, and J. Zaanen, Phys. Rev. Lett. **108**, 106403 (2012).
 - [8] T. L. Hughes, H. Yao, and X.-L. Qi, Phys. Rev. B **90**, 235123 (2014).
 - [9] R.-J. Slager, A. Mesaros, V. Juričić, and J. Zaanen, Phys. Rev. B **90**, 241403(R) (2014).
 - [10] Y. You, G. Y. Cho, and T. L. Hughes, Phys. Rev. B **94**, 085102 (2016).
 - [11] R.-J. Slager, V. Juričić, V. Lahtinen, and J. Zaanen, Phys. Rev. B **93**, 245406 (2016).
 - [12] H. Hamasaki, Y. Tokumoto, and K Edagawa, Appl. Phys. Lett. **110**, 092105 (2017).
 - [13] A. K. Nayak, J. Reiner, R. Queiroz, H. Fu, C. Shekhar, B. Yan, C. Felser, N. Avraham, and H. Beidenkopf, Sci. Adv. **5**, eaax6996 (2019).
 - [14] R. Queiroz, I. C. Fulga, N. Avraham, H. Beidenkopf, and J. Cano, Phys. Rev. Lett. **123**, 266802 (2019).
 - [15] T. Nag and B. Roy, Commun. Phys. **4**, 157 (2021).
 - [16] B. Roy and V. Juričić, Phys. Rev. Research **3**, 033107 (2021).
 - [17] A. Panigrahi, R. Moessner and B. Roy, Phys. Rev. B **106**, L041302 (2022).
 - [18] A. Panigrahi, V. Juričić and B. Roy, Commun. Phys. **5**, 230 (2022).
 - [19] S. Velury and T. L. Hughes, Phys. Rev. B **105**, 184105 (2022).
 - [20] S. K. Das and B. Roy, arXiv:2210.15661
 - [21] S. K. Das, S. Manna, and B. Roy, arXiv:2211.09804
 - [22] N. H. Lindner, G. Rafael, and V. Galitski, Nat. Phys. **7**, 490 (2011).
 - [23] B. Dóra, J. Cayssol, F. Simon and R. Moessner, Phys. Rev. Lett. **108**, 056602 (2012).
 - [24] M. S. Rudner, N. H. Lindner, E. Berg, and M. Levin, Phys. Rev. X **3**, 031005 (2013).
 - [25] A. Eckardt, Rev. Mod. Phys. **89**, 011004 (2017).
 - [26] T. Oka and S. Kitamura, Ann. Rev. Cond. Mat. Phys. **10**, 387 (2019)
 - [27] See Supplementary materials at XXX-XXXX for metallic state along large angle grain boundary and details of the Floquet Hamiltonian.
 - [28] X.-L. Qi, Y.-S. Wu, and S.-C. Zhang, Phys. Rev. B **74**, 085308 (2006).
 - [29] D. J. Thouless, M. Kohmoto, M. P. Nightingale, and M. den Nijs, Phys. Rev. Lett. **49**, 405 (1982).

- [30] T. Fukui, Y. Hatsugai, and H. Suzuki, *J. Phys. Soc. Jpn.* **74**, 1674 (2005).
- [31] H. F. Trotter, *Proc. Amer. Math. Soc.* **10**, 545 (1959).
- [32] M. Sujuki, *Commun. Math. Phys.* **51**, 183 (1976).
- [33] Y. H. Wang, H. Steinberg, P. Jarillo-Herrero and N. Gedik, *Science* **342**, 453 (2013).
- [34] M. Tarnowski, F. N. Ünal, N. Fläschner, B. S. Rem, A. Eckardt, K. Sengstock and C. Weitenberg, *Nat. Commun.* **10**, 1728 (2019).
- [35] K. Wintersperger, C. Braun, F. N. Ünal, A. Eckardt, M. D. Liberto, N. Goldman, I. Bloch and M. Aidelsburger, *Nat. Phys.* **16**, 1058 (2020).
- [36] M. C. Rechtsman, J. M. Zeuner, Y. Plotnik, Y. Lumer, D. Podolsky, F. Dreisow, S. Nolte, M. Segev and A. Szameit, *Nature (London)* **496**, 196 (2013).
- [37] L. J. Maczewsky, J. M. Zeuner, S. Nolte and A. Szameit, *Nat. Commun.* **8**, 13756 (2017).
- [38] Q. Cheng, Y. Pan, H. Wang, C. Zhang, D. Yu, A. Gover, H. Zhang, T. Li, L. Zhou and S. Zhu, *Phys. Rev. Lett.* **122**, 173901 (2019).
- [39] S. Afzal, T. J. Zimmerling, Y. Ren, D. Perron and V. Van, *Phys. Rev. Lett.* **124**, 253601 (2020).
- [40] R. Fleury, A. B. Khanikaev and A. Alu, *Nat. Commun.* **7**, 11744 (2016).
- [41] Y-G. Peng, C-Z. Qin, D-G. Zhao, Y-X. Shen, X-Y. Xu, M. Bao, H. Jia and X-F. Zhu, *Nat. Comm.* **7**, 13368 (2016).
- [42] H. W. Kim, S-H. Kang, H-J. Kim, K. Chae, S. Cho, W. Ko, S. H. Kang, H. Yang, S. W. Kim, S. Park, S. W. Hwang, Y-K. Kwon, Y-W. Son, *Nano Lett.* **20**, 5837 (2020).
- [43] F.-F. Li, H.-X. Wang, Z. Xiong, Q. Lou, P. Chen, R.-X. Wu, Y. Poo, J.-H. Jiang, and S. John, *Nat. Comm.* **9**, 2462 (2018).
- [44] I. H. Grinberg, M. Lin, W. A. Benalcazar, T. Hughes and G. Bahl, *Phys. Rev. Applied* **14**, 064042 (2020).